A NEW METHOD FOR DEFECTS DETECTION IN CFRP COMPOSITES USING WAVELET ANALYSIS AND NON-CONTACT LAMB WAVES PROPAGATION

Léa A.C. Lecointre,[1] Ryo Higuchi,[1] Tomohiro Yokozeki,[1] Shota Tonegawa,[2] Masakatsu Mita,[2] Naoki Hosoya,[2] and Shin-ichi Takeda,[3]

[1] Department of Aeronautics & Astronautics, The University of Tokyo, Japan
[2] Department of Engineering Science & Mechanics, Shibaura Institute of Technology, Tokyo, Japan
[3] Aeronautical Technology Directorate, Japan Aerospace Exploration Agency (JAXA), Mitaka, Japan

Abstract: The use of Lamb Waves for Ultrasonic Testing (UT) has been shown in the past decades as a very promising lead for the improvement of the Non-Destructive Testing (NDT) of wide parts such as spacecraft or aircraft parts. However, the mastery of Lamb Waves propagation in highly anisotropic and layered materials such as Carbon Fiber Reinfored Plastics (CFRP), as well as the mastery on non-contact excitation of Lamb Waves, are still limitations to the implementation of such methods for real life applications.
In this study, we are investigating the ability to detect defects with a recently developed system for non-contact Lamb Waves excitation based on a Laser Induced Plasma Shock Wave (LIPSW) generation. In order to detect artificial delamination, we are developing a novel Signal Processing algorithm which is based on a Wavelet Transform analysis in order to generate Probability Functions of defects presence. The experimental results demonstrated the possibility to detect wide and small artificial delamination. A quantitative analysis shown that the current method is not as precise as classic Ultrasonic methods yet, but opens new leads for the development of efficient fully non-contact NDT system based on Lamb Waves propagation.

Keywords: Non-Destructive Testing, Ultrasonic Testing, Lamb Waves, CFRP, Wavelet Analysis

INTRODUCTION

Ultrasonic Testing (UT) has been shown over the years both in industry and in research as the most efficient method for the Non-Destructive Testing (NDT) of Carbon Fibers Reinforced Plastic (CFRP) structures, which are widely used in aerospace and aeronautical fields due to their great mechanical properties associated with a low weight. However, most UT methods still show some limitations for aerospace industry, in particular the necessity to scan full parts which is highly time-consuming and can be challenging for example in the case of maintenance of mounted aircraft parts. For these reasons, the use of Lamb Waves for the detection of defects in CFRP has been widely investigated numerically and experimentally over the past decades by researchers [1-4].

Among the main research leads investigated for the implementation of Lamb Waves methods for NDT, the development of non-contact generation systems is of utmost importance as it may provide promising NDT systems for the control of aerospace structures in real life applications. Methods involving Air-Coupled Transducers have been investigated [5], as well as systems based on thermal expansion induced by laser [6-8], however, the amplitude of excited Lamb Waves is relatively small. Another method have been shown as able to excite Lamb Waves: the Laser Ablation, in which a plasma plume is excited at the surface of a material with a high pulse laser [9,10]. This method is not applicable to NDT purposes as it slightly damages the surface of the structure. More recently, a new non-contact method using the shock wave generated by a plasma plume, excited a few centimetres on top of a sample in order to avoid structural damage, has been shown as able o generate Lamb Waves by Hosoya et al. [11]. This method can be referred to as a Laser Induced Plasma Shock Wave (LIPSW) system and is particularly promising as it allows to generate wide frequency band and relatively high amplitude waves. However, due to these particular features, adapted Signal Processing methods have to be developed in order to apply this method to defects detection.

Signal Processing is another important lead of research for the development of Lamb Waves based NDT methods, and several types of algorithms have been developed for defects detection [12,13]. In particular, the Wavelet Transform has been shown as particularly efficient for the characterisation of Lamb Waves as it allows to visualise signals in time and frequency domains [14,15].

In this study, a LIPSW system is used to experimentally generate Lamb Waves in several CFRP samples, some including artificial delamination. In order to investigate the ability to detect these delaminations, a novel Signal Processing algorithm is developed with using a Wavelet Analysis of the experimental signals combined with Image Processing tools to generate defects presence probability functions. Then, the results are quantitatively analysed and compared with classic NDT method commonly used for CFRP control. In the second part of this document, the experimental set-up and samples are described. In the third part, the development of the Signal Processing algorithm is detailed. Finally, the experimental results are presented and discussed in the fourth part.

PART I: EXPERIMENTAL METHODOLOGY

This study employs a fully non-contact system to excite and measure the propagation of Lamb Waves. The excitation system is based on a Laser Induced Plasma Shock Wave (LIPSW). In this method, a high pulse laser beam is focalised by a plano-convex lens at a distance d from the surface of the experimental sample. The generation of Laser Induced Plasma induces a shock wave which, when propagating through the air, encounters the surface of the sample, starting then the Lamb Waves excitation within it. The measurement system is a Scanning Laser Doppler Vibrometer (SLDV), which uses frequency change due to the Doppler effect to measure surface vibrations. Therefore, the measurement of Lamb Waves propagation relies on the displacement-time data recorded by the SLDV at any point of the surface of the experimental sample.

Two different configurations can be used for this experiment. In the “same side” configuration, the generation of the Lamb Waves and the measurement of surface vibration are performed on the same side of the sample. Studying this configuration is useful in order to adapt the method to real-life aerospace applications in which the control sometimes has to be performed on mounted aircraft parts which both sides are not accessible by the operator. However, the disadvantage of this configuration is that the shock wave hits all the surface of the sample after generating the Lamb Waves propagation at the excitation point. Therefore, the shock wave signal is detected by the SLDV and must be differentiated from Lamb Waves propagation during the Signal Processing analysis. The “opposite side” configuration used a system in which the SLDV measurement and the LIPSW excitation are performed on different sides of the sample. This method facilitates the Signal Processing because the Shock Wave hit on the sample after Lamb Waves excitation does not appear in the SLDV measured data, but it is important to note that it more difficult to adapt to many real-life applications. In the figure 1, both experimental configurations are schematized for better understanding.

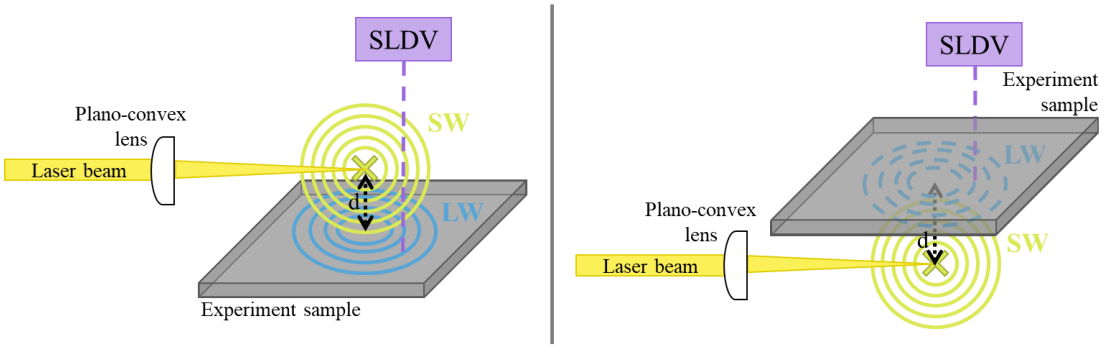

(a) « Same side » configuration (b) « Opposite side » configuration

Figure 1: Representation of the experimental set-up in the two configurations developed

The samples investigated in this study are quasi-isotropic laminates of various thicknesses and including various types of delamination. They can be split into two main groups: the "stiffened samples" LW-08-08-00, LW-08-08-50S and LW-08-08-75S which include a stiffened zone at the center and allow to investigate the detection of wide delamination zones, and the "small delamination samples" LW-16-00-siz and LW-32-00-dep which are flat samples including small round shaped artificial delaminations with various sizes (10-mm, 30-mm and 50-mm) and depths (8-ply depth or shallow, 16-ply depth or mid-plane and 24-ply depth or deep). The material parameters are presented in the table 1. The samples geometry is detailed in the figure 1 and the table 2.

Table 1: Material parameters of the experimental samples.

E1 [GPa]	*E2 [GPa]*	*v12 [GPa]*	*v23 [GPa]*	*G12 [GPa]*	*G23 [GPa]*	*Density [kg/m^3]*	*Ply thickness [mm]*
152	8.0	0.34	0.54	4.03	2.52	1539	0.2

Table 2: Detailed features of the experimental samples. The elements written in brackets refer to the stiffened zone of stiffened samples.

Type	*Sample denomination*	*Ply number*	*Thickness [mm]*	*Lay-up*	*Condition*
"Stiffened samples"	LW-08-08-00	8 (16)	1.6 (3.2)	[45/0/-45/90]s (+[-45/90/45/0])	Healthy, stiffened
	LW-08-08-50S	8 (16)	1.6 (3.2)	[45/0/-45/90]s (+[-45/90/45/0])	Delaminated, stiffened
	LW-08-08-75S	8 (16)	1.6 (3.2)	[45/0/-45/90]s (+[-45/90/45/0])	Delaminated, stiffened
"Small delamination samples"	LW-16-00-siz	16	3.2	([45/0/-45/90])2	Delaminated, flat
	LW-32-00-dep	32	6.4	([45/0/-45/90])2	Delaminated, flat

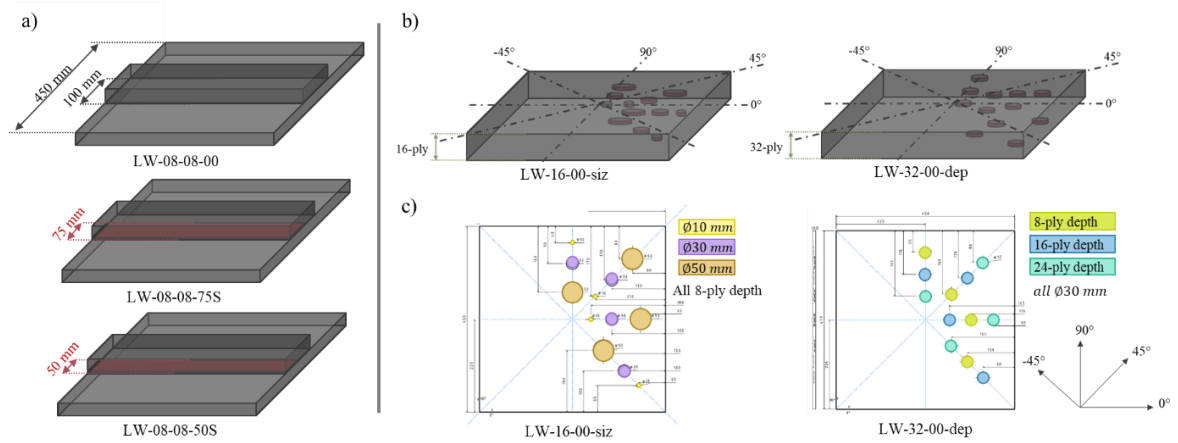

Figure 2: Detailed view of the experimental samples geometry. Delamination zones appear in red in the 3D views. a) 3D views of stiffened samples. b) 3D view of small delamination samples. c) 2D view of small delamination samples with artificial defects placement details.

PART II: SIGNAL PROCESSING ALGORITHM

Data acquisition

The measurement of Lamb Waves propagation in the samples in the objective of detecting the defects is performed by using an SLDV. The vibrometer records the out-of-plane displacement of the surface particles during a recording time t_{max} and with a sampling frequency F_s.The principle challenge for the signal processing of the experimental Lamb Waves excited by a LIPSW system is that the shock wave excitation generates a Lamb Waves propagation which gathers a wide frequency range. This fact, added to the dispersive nature of Lamb Waves, makes the propagation particularly complex to process. In order to keep enough information to exploit on one hand while obtaining a reasonable Signal to Noise Ratio (SNR) and making the Signal Processing possible on the other hand, a passband filter is applied to every measured signal. These data acquisition features are adapted to both samples natures (stiffened samples and small delamination samples) and summarized in the table 3.

Table 3: Data acquisition parameters for the two types of samples

Sample type	*Sample denomination*	*Recording time t_{max} [µs]*	*Sampling frequency F_s [MHz]*	*Time samples T_S*	*Passband filter [kHz]*
"Stiffened samples"	LW-08-08-00	800	2.56	2048	[8 – 600]
	LW-08-08-50S	800	2.56	2048	[8 – 600]
	LW-08-08-75S	800	2.56	2048	[8 – 600]
"Small delamination samples"	LW-16-00-siz	1600	3.125	5000	[10 – 600]
	LW-32-00-dep	1600	3.125	5000	[10 – 600]

The measurement zone on the stiffened samples is a 200x200 mm squared area centered on the plate with one measurement point every 2 mm, which corresponds to a total of 10201 points measured, or 10201 signals composed of 2048 time samples. Therefore, the experimental raw data takes the form of a matrix containing 10201 columns and 2048 rows. The signal measured at each point is averaged 10 times, which takes about 1s of measurement. Therefore, the total duration of measurement took around 3 hours. However, this time can easily be reduced by reducing the number of averages.

The small delamination samples were measured with only 3 averages for each point and the SNR stayed satisfying. The measurement zone, due to the localisation of artificial defects, was wider: 400x400 mm area with measurement points every 2 mm, which gives a number of 40401 points. 5000 time samples were taken in order to visualise the waves reflected from the plate boundaries. Therefore, the raw experimental data took the form of a matrix containing 40401 columns and 5000 rows. As the number of averages was reduced, the experimental time was around 4 hours.

Signal Processing flowchart

During the investigation of experimental results, it has been observed that despite the Lamb Waves propagation seems to differ in defects areas from healthy areas, it is not possible to identify defect areas without comparison with healthy areas. Therefore, the raw data matrices have been divided into matrices containing signals propagating in healthy zones, called “baseline” matrices and matrices containing signals propagating in defected zones, called “control-line” matrices. The baseline matrix for stiffened samples is simply the matrix measured on the sample LW-08-08-00 which has the same structure than the two other samples but does not contain delamination. The two matrices obtained from the propagation in LW-08-08-50S and LW-08-08-75S are control-line matrices which will be compared to the corresponding baseline matrix.

In the case of small delamination samples, the zone of each sample which do not contain any defect has been used a baseline, while the zone containing defects has been used as control-line. Therefore the raw data matrices are divided by two, which gives two matrices of size 20200x5000 for each sample. The comparison of the control-line matrices with corresponding baseline matrices is obviously performed with symmetry to the center of the plate in order to take consideration of the fibers direction.
The allocation of each measured zone for each sample into baseline or control-line matrix is schematized in the figure 3.

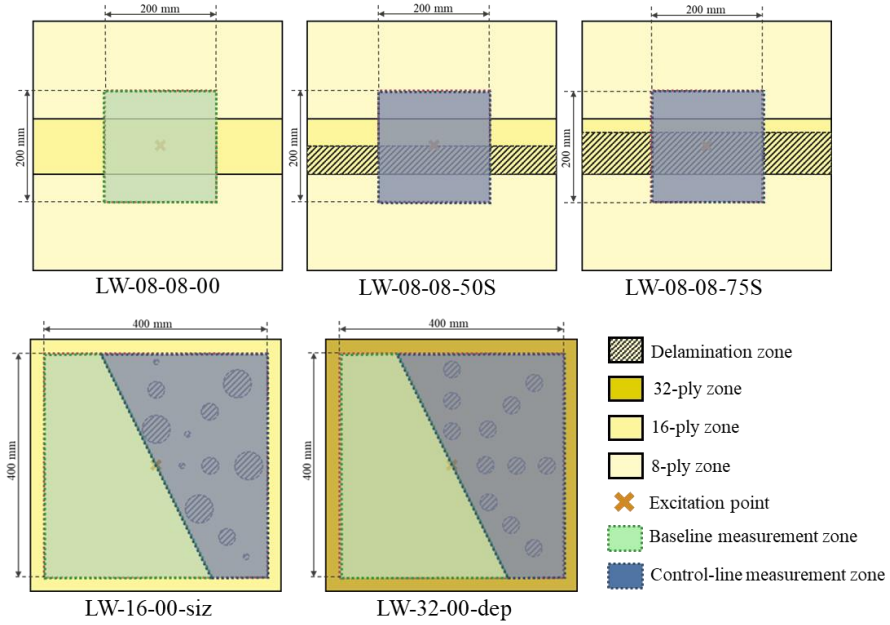

Figure 3: Allocation of the measurement zones as baseline or control-line matrices for each sample.

The principle of the Signal Processing algorithm is to process the raw experimental matrices to obtain at the end a Probability Function at every measurement point of the sample which gives an index between 0 and 1 assessing the probability of presence of a defect. This means that by plotting the Probability Function in a spatial 2D cartography of the surface points, the defects localisation should be obtained, and the result can be easily compared to classic NDT methods providing 2D spatial information such as a ultrasonic C-scan. In order to obtain the Probability Functions, the algorithm consists in two main steps. In the first step, the raw experimental data are treated using a Wavelet Transform, and then the data points are spatially localised, in order to obtain at the end of the first step

extended matrices which include multi-domain information of the Lamb Waves propagation in the measured zone. The matrices at the end of this step are 3D matrices including information of the signal in the time-domain, the frequency-domain and the spatial-domain.

The second main step of the algorithm is to extract different information from the 3D data matrices and to treat these information by comparison between baselines and control-lines in order to obtain various Damage Indexes (DIs). The DIs are then weighted in order to form the final Probability Functions by using a genetic algorithm for obtaining the best optimization. Two main methods are used in order to obtain DIs. The first method consists of removing the 3D matrix of baseline from the 3D matrix of control-line, and then to extract information from the resulting 3D matrix (which contains only the absolute difference from baseline and can therefore be attributed to the presence of defects). The second method consists in extracting information from the baseline 3D matrix and from the control-line 3D matrix and to use Image Processing tools in order to calculate DIs from image comparison of the baseline and the control-line. The general flow chart of the Signal Processing algorithm is represented in figure 4 and will be detailed step-by-step in the following paragraphs.

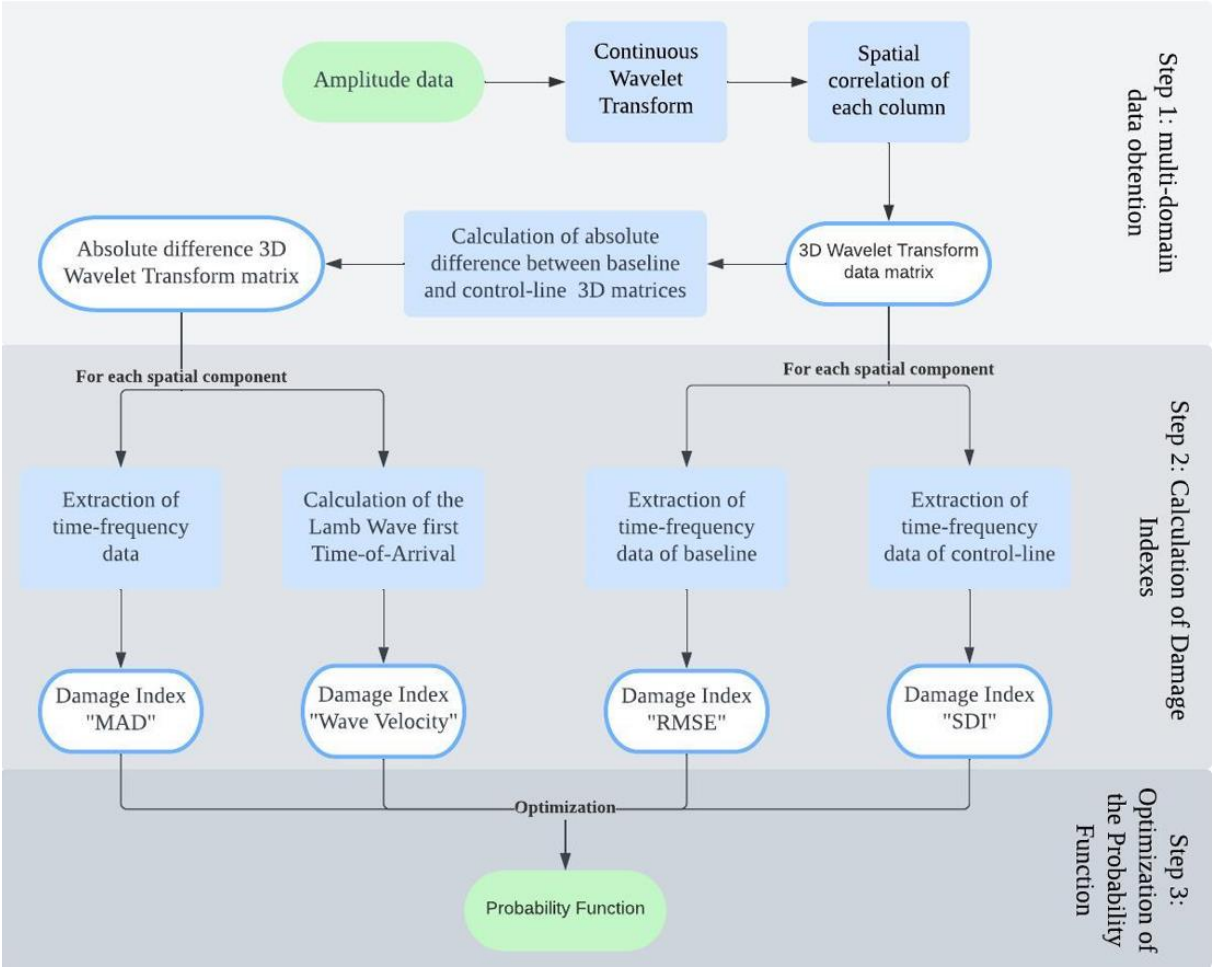

Figure 4: General flow chart of the Signal Processing algorithm.

The Wavelet Transform

The first step of Signal Processing involved the principle of Wavelet Transform analysis in order to generate 3D matrices containing extended information about the experimental wave propagation. The continuous Wavelet Transform is applied over a loop on each signal measured. For each signal, a coefficient cwt (coefficient of wavelet transform) is calculated as:

$$cwt(t,s) = \frac{1}{\sqrt{s}} \int \Psi^* \frac{(t-\tau)}{s} x(t) dt \quad (1)$$

Where τ and s are the time and scaling factors, which allow to evaluate the signal in the time-domain and the frequency-domain respectively, x(t) is the signal analysed and $\Psi^*$is the complex conjugate of the mother wavelet Ψ which, in this study, is a Morse wavelet. Then, a spatial correlation is performed in order to correlate each analyse point to its distance from the point of excitation. Therefore, at the end of the first step, the extended matrix which is referred to as "3DWT matrix" is a matrix of size $f \times T_S \times P$ with f the number of frequency components generated during the Wavelet Transform, T_S the number of time simples for the measurement of each signal and P the number of points at which the signal is measured, each of these point being located at a distance D from the excitation point. The table 4 gives the values of these parameters for each 3DWT matrix.

Table 4: Details on the 3D WT matrix for each baseline and control-line studied.

Matrix denomination	*Measurement zone (Cf. Figure 3)*	*Matrix size*		
		f	T_S	P
3DWT_LW08_BL	200x200 square at the center of LW-08-08-00	81	2048	10201
3DWT_LW08_50S	200x200 square at the center of LW-08-08-50S	81	2048	10201
3DWT_LW08_75S	200x200 square at the center of LW-08-08-75S	81	2048	10201
3DWT_LW16_BL	Healthy zone of LW-16-00-siz	94	5000	20200
3DWT_LW16_CL	Defected zone of LW-16-00-siz	94	5000	20200
3DWT_LW32_BL	Healthy zone of LW-32-00-dep	94	5000	20200
3DWT_LW32_CL	Defected zone of LW-32-00-dep	94	5000	20200

Obtention of Damage Indexes

The second main step of the Signal Processing algorithm consists in calculating DIs extracted from the 3D WT matrices. Two main types of DIs are considered: (i) DIs extracted from a 3D WT matrix containing only the absolute difference data between baseline and control-line and (ii) DIs calculated by comparison of images extracted from baselines and control-lines using Image Processing tools. The DIs calculated using the first method (i) are the "MAD" and the "Wave velocity". The DIs calculated using the second method (ii) are the "RMSE" and the "SDI".

- "MAD" Damage Index

The DI "MAD" (for Mean Absolute Difference) reflects the absolute difference between the cwt for the baseline and the control-line at each measurement point. The 3D WT matrix of baseline and control-line are firstly subtracted in order to generate a new 3D matrix containing only the absolute difference of cwt. Then, the cwt value for all frequency components and all time samples is averaged at each point. Finally, this mean cwt value at each point is normalized by the maximum mean cwt value in order to obtain an "MAD" index between 0 and 1 with higher mean cwt (which reflects a larger wave absolute amplitude and/or a wider frequency bandwidth) closer to 1 and lower mean cwt closer to 0. The punctual outlier values (exceeding three standard variations from the mean) are automatically replaced using the MATLAB function "filloutliers". Finally, the "MAD" DIs which have been obtained at each point of the measured area can be plotted in spatial 2D by using the spatial data of the points in order to see a cartography of "MAD" index. The 2D spatial visualization of "MAD" for each experimental sample are shown in the figure 5. The higher "MAD" values are obtained in defected zones for each sample, which is a good outcome for defects detection. However, some limitations to this DI efficiency are also to be noted:

- In the “stiffened samples”, the healthy zone which is located below the delamination has “MAD” values up to around 0.7, which is too high for a healthy zone. This is assumed to be due to a mismatch between the baseline (healthy plate which does not contain any delamination) and control-lines. After crossing the delamination, the wave propagation in the healthy zone is not comparable to wave propagation which do not cross any delamination.
- In the “stiffened samples”, the delaminated zone which is located in the horizontal band from 50 to 100 mm and from 50 to 125 mm for LW-08-08-50S and LW-08-08-75S respectively contains the higher “MAD” values but is not homogeneous enough, some zones in the delaminated band show “MAD” values under 0.5 which is too low.
- In the “small delamination samples”, the healthy zones in the control-line “MAD” values are around 0.4, which is quite high for healthy zones and can lead to misdetection or confusion when attempting to detect defects. As a comparison, the baseline zone on the left part of the cartographies is shown with 0 “MAD” value and the colour difference is considerable.
- In the “small delamination samples”, the excitation zone located at the centre of the cartography shows “MAD” values up to 0.8 which is too high and can lead to wrong defect indication. On the contrary, the defect zones despite they show higher values of “MAD” are not accurately enough detected. In the case of LW-32-00-dep, it is clear that the “MAD” Damage Index is highly sensitive to the depth of the defects as the values are higher in shallow defects and lower in deeper defects.

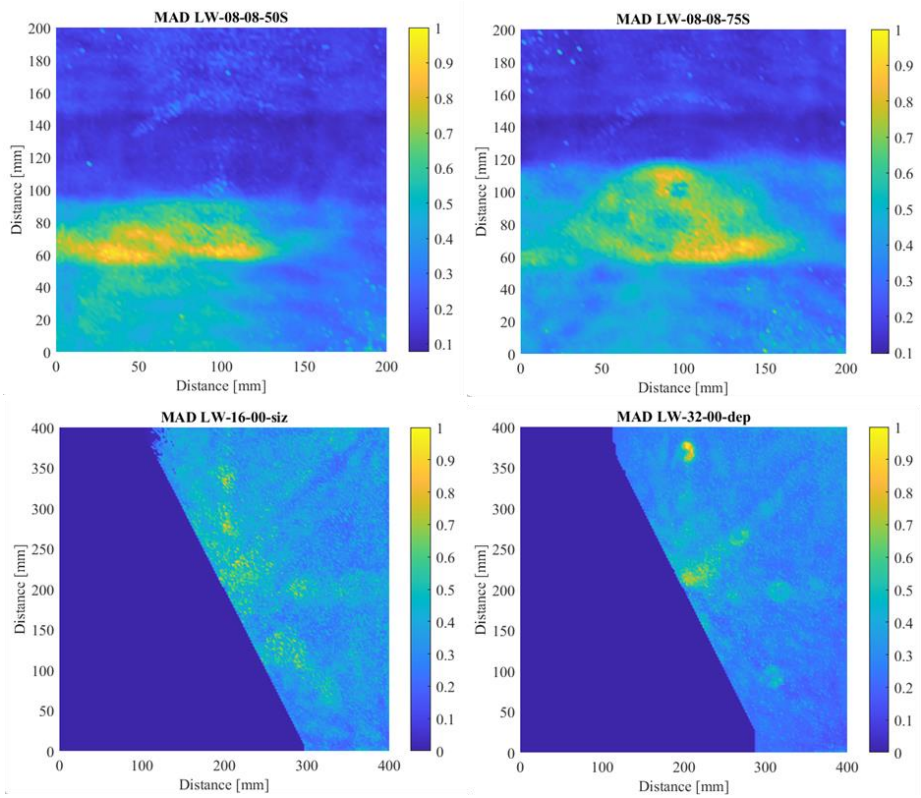

Figure 5: Visualisation of the “MAD” indexes results for all experimental samples

- “Wave velocity” Damage Index

In order to calculate the wave energy velocity, the time of arrival of the largest frequency band of the Lamb Wave signal is recorded at each point of measurement. This time of arrival is then transformed into wave velocity by dividing it from the distance from excitation. The wave velocity value obtained are then displayed in spatial 2D cartographies, as shown in the figure 6. It is observed that in the case of “stiffened samples”, higher Wave velocity values are obtained in the delaminated zones, in particular in the case of LW-08-08-75S. However, the delaminated zones are not fully detected, some higher wave velocity values are obtained in the healthy zone located below the delaminations, and two main wrong indications are observed: (i) the excitation zone, which is due to the shock wave effect and (ii) the zone

at geometry change above the delamination. In the "small delamination samples", the wave velocity did not allow to visually detect the defects. It is observed that the wave velocity values are relatively homogeneous in the fibres directions and more disturbed in the healthy zones. Therefore, this DI as it is calculated in the current study is shown to be not adapted for the detection of small delamination.

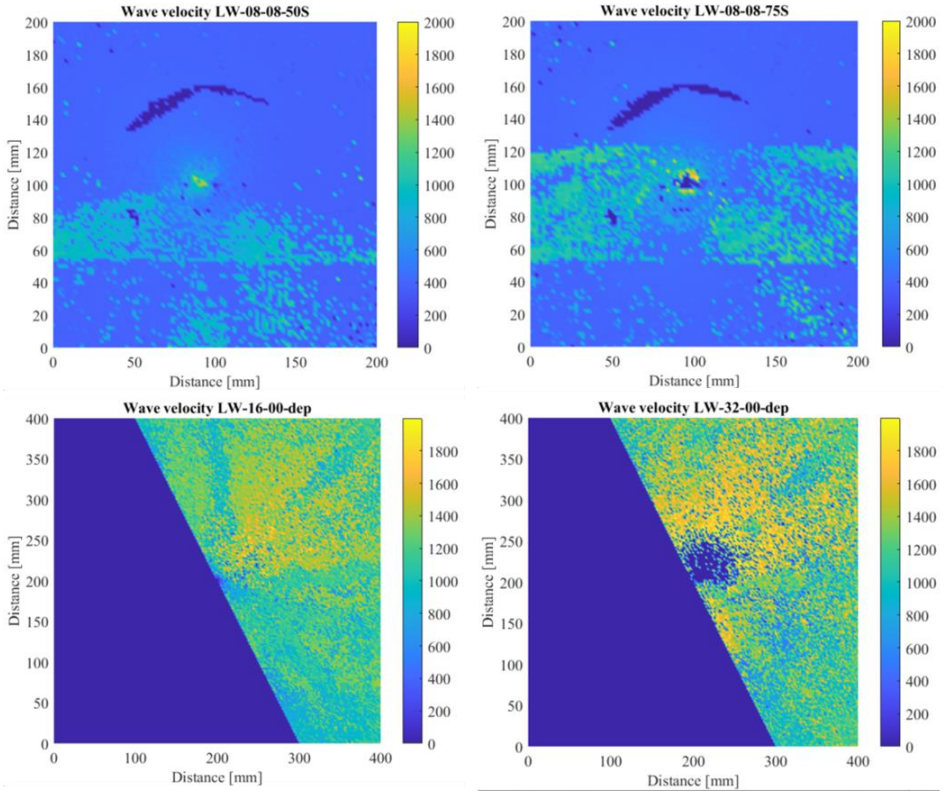

Figure 6: Visualisation of the "Wave Velocity" results for all experimental samples

- "RMSE" Damage Index

Another method for calculating DIs from the 3D WT matrices is to use Image Processing algorithms for the comparison of extracted images from the baselines and the control-lines.

The "RMSE" Damage Index calculates the Root Mean Squared Error of time-frequency images extracted from the baseline and the control-line at each point of measurement. The RMSE calculates the squared error level between every point of two images, therefore RMSE is highly sensitive to any difference between the to images:

$$RMSE(X) = \sqrt{\frac{1}{n}\sum_{i=1}^{n}(i_{baseline} - i_{control\ line})^2}, \quad (2)$$

With n the number of points i investigated (in the case of time-frequency images n is 81x2048 and 94x20200 for stiffened samples and small delamination samples respectively) and X the point localisation or distance from excitation in the case of time-frequency images.

Then, the RMSE index is normalized by the maximum RMSE value collected and the outlier values are replaced using the same method as for "MAD" index. The RMSE results are shown in the figure 7. The RMSE cartographies are comparable to the MAD ones, which is expected due to the nature of both calculation methods. As for the "MAD" index, the dependency of RMSE to any slight image difference lead to high values even in some healthy zones such as the zone below delamination in the stiffened samples. However, the highest values of RMSE are observed in the defected zones which is a satisfying outcome for defects detection possibility.

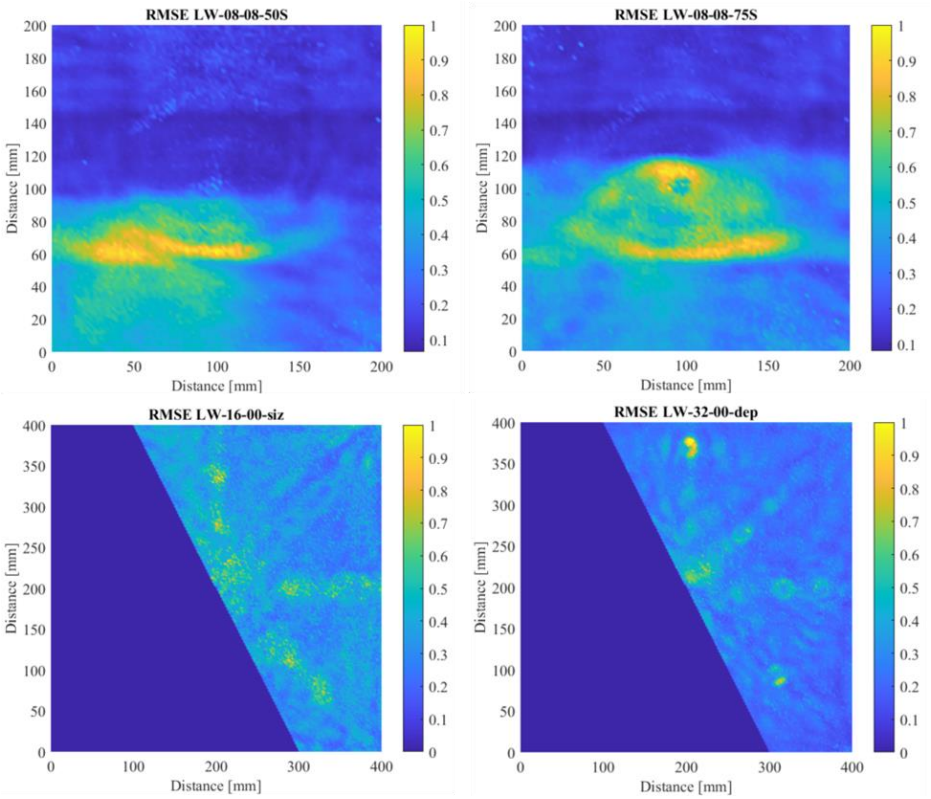

Figure 7: Visualisation of the "RMSE" indexes results for all experimental samples

- "SDI" Damage Index

Another way to use Image Processing for the comparison of images extracted from baselines and control-lines is to use a Structural Dissimilarity Index (SDI) between the two images. The SDI does not consider the difference between baseline and control-line at each single point of the images but generates an index which reflects the main structural differences between the two images based on three characteristics: the images contrast, the images luminance and the images structure. Therefore, SDI is less sensitive to small punctual differences due to measurement inaccuracies and highlights real changes due to wave propagation differences (different wave amplitude, different time of arrival and different frequency bandwidth). The SDI is calculated using the equation:

$$SDI = \frac{1}{2}\big(1 - l(BL, CL) \times c(BL, CL) \times s(BL, CL)\big), \tag{3}$$

with $l(BL, CL), c(BL, CL)$ and $s(BL, CL)$ respectively the luminance comparison, contrast comparison and structure comparison indexes between the baseline image BL and the control line image CL, calculated by

$$l(BL, CL) = \frac{(2\mu_{BL}\mu_{CL} + c_1)}{\left(\mu^2{}_{BL} + \mu^2{}_{CL} + c_1\right)}, \tag{4}$$

$$c(BL, CL) = \frac{(2\sigma_{BL}\sigma_{CL} + c_2)}{(\sigma^2{}_{BL} + \sigma^2{}_{CL} + c_2)}, \tag{5}$$

$$s(BL, CL) = \frac{(cov_{BLCL} + c_3)}{(\sigma_{BL}\sigma_{CL} + c_3)}, \tag{6}$$

with for each image μ the pixel sample mean and σ the variance, cov the covariance between the two images, and c_1, c_2 and c_3 stabilization parameters depending on the dynamic range of image pixels values. The SDI results are displayed in the figure 8. The lower sensitivity of SDI to small punctual variations between the baseline and the control-line is confirmed by observing the images: healthy zones SDI values are closer to 0, which is a good outcome as is allows to enhance the contrast between healthy

zones and defected zones and therefore clarifies the defects detection. Some limitations already pointed out with the other DIs are however retrieved:

- The healthy zone located below the delamination in the stiffened samples has a too high SDI value, which can lead to wrong defects indication. As mentioned before, this issue is assumed to be due to a mismatch between the baseline and the control-lines, therefore adaptation of the baseline in future investigations is considered as a promising lead to solve the problem.
- The detection of small defects in small delamination samples is inaccurate, the sizing of these small defects being underestimated and some defects being undetected. In the case of LW-32-00-dep, this leads to a clear indication that the method is highly sensitive to the defects depth. Overall, these results indicate that the method seems to have defects size and depths detectability conditions which will be quantified in future investigations.
-

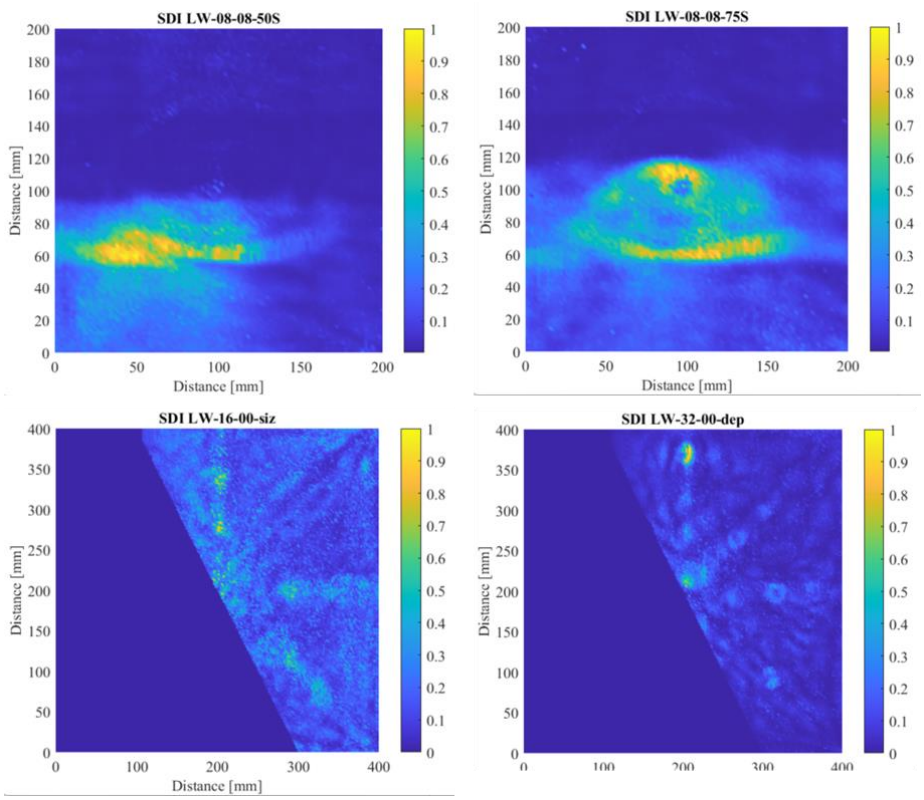

Figure 8: Visualisation of the "SDI" indexes results for all experimental samples

Optimization of the Probability Function

From the calculated DIs, a probability function which gives an index of defect presence between 0 and 1 is calculated. In order to weight every DI, a genetic algorithm is used for minimizing the difference between the Probability Function PF2 defined as:

$$PF2 = \frac{1}{4}\left(\alpha\frac{RMSE}{RMSE_{max}} + \beta\frac{SDI}{SDI_{max}} + \gamma\frac{MAD}{MAD_{max}} + \varepsilon\frac{velocity}{velocity_{max}}\right), \quad (8)$$

with α,β,γ and ε all between 0 and 1 and their sum being equal to 1. And a reference value of 0 for healthy zones and 1 for defected zones for each sample. For every sample, the genetic algorithm optimization indicates that the indexes α, γ, and ε tend to 0 while β tends to 1. This confirms that SDI is the best DI to detect the artificial defects, which was already expected from the 2D spatial cartographies of each DI.

PART III: RESULTS & DISCUSSION

Stiffened samples results

The qualitative (spatial cartographies) and quantitative (DIs average values in different zones) experimental results of the stiffened samples are shown in the figure 9 with a) and b) the quantitative results and c) and d) the qualitative results of LW-08-08-50S and LW-08-08-75S respectively. In the figure 9 a) and b), the quantitative results from DIs calculation are compared with a reference value which is the normalized dB attenuation measured from an ultrasonic C-scan in transmission mode. The error bars represent the standard deviation of the normalized values in the considered zone.

Due to the important discrepancy of the DIs values in the different zones of the samples, the standard deviation is relatively high in most zones and for most DIs, which is an important limitation of the method compared to the reference method C-scan which standard deviation is better. The only exceptions are in the upper 8-ply zone and the 16-ply zone which are very similar in the baseline sample LW-08-08-00 and in the control-line samples. Therefore, it is assumed that an improvement of the baseline would be an interesting lead to solve this issue.
For every DI including the reference method, the mean index value recorded in the delaminated zone is always higher than the mean index recorded in the healthy zones and in the full plate. However, it is interesting to note that in the case of the reference method, there is a minimum of about 50% difference between the delaminated zone value and the healthy zones values. This difference level is an important element for purposes of NDT as the visual contrast between defects and healthy zones is fundamental for the defects detection. In most DIs calculated in the current study, this 50% level is not reached, except in the case of SDI, which was pointed out as the better method from the optimization as explained in the previous part.

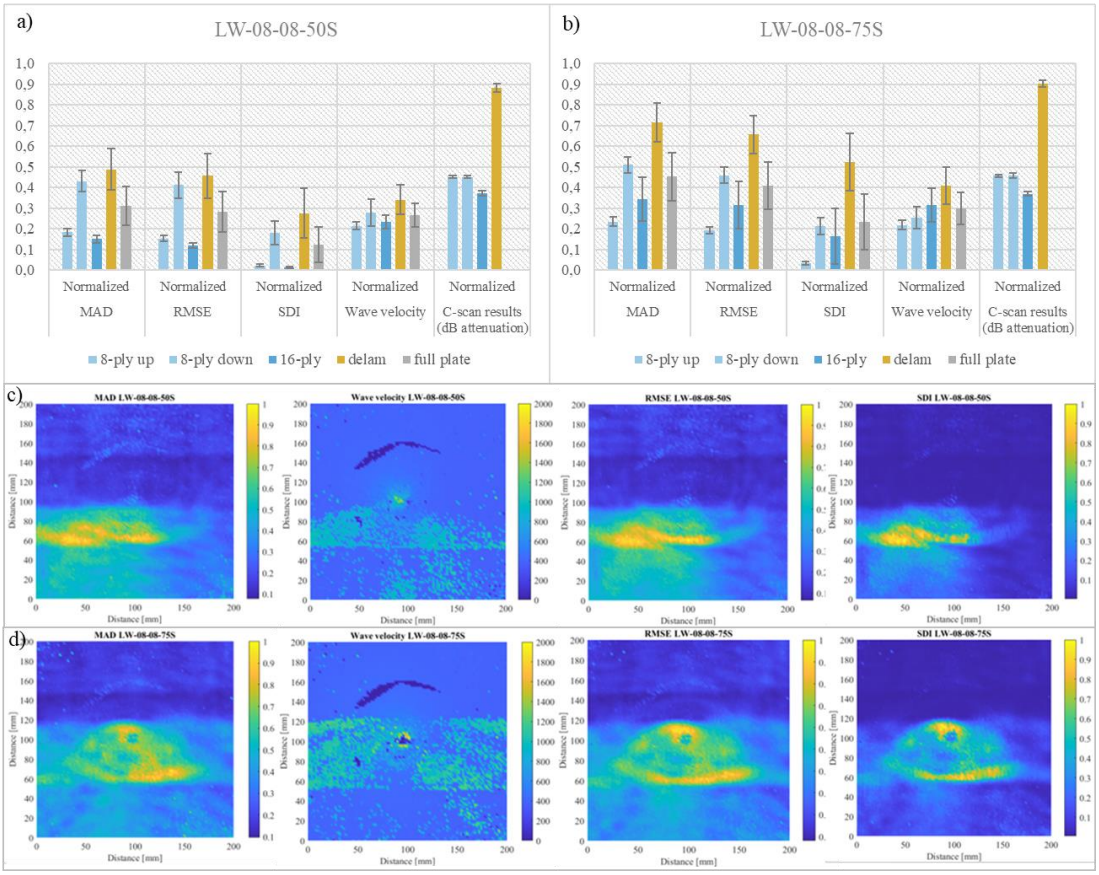

Figure 9: a) Quantitative and b) Qualitative results for stiffened samples

Small delamination samples results

The quantitative and qualitative results of small delamination samples are presented in the figures 10 and 11. In the case of small delamination samples, the quantitative analysis does not compare healthy zones with delaminated zones but each defect results with the full control-line. In the figure 10 a), the normalized DIs calculated for each defect zone is represented using the same colours than in figure 2 for each defect size, and the direction of the bin pattern recalling the fibre direction on which the defect is located. The legend lists the defects in the same order than appearing on the graph, from left to right. In the figure 10 b), the 2D spatial cartographies obtained for each DI are shown with an indication of the real localisation of the artificial defects and the fibres directions in white dashed lines.

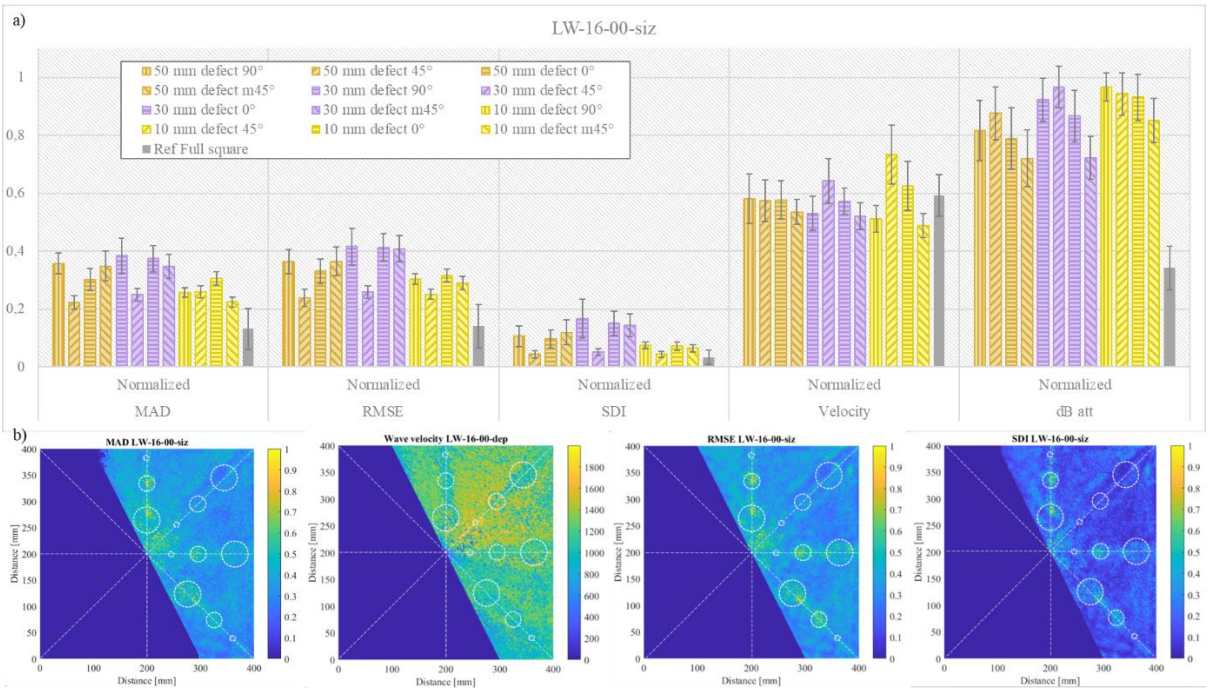

Figure 10: a) Quantitative and b) Qualitative results for LW-16-00-siz

The quantitative results confirm that the sizing of small defects is currently not accurate enough for ensuring reliable defects detection. It is firstly confirmed with the important difference of mean values between defects between the calculated DIs and the reference C-scan DI. Moreover, as it was mentioned in the analysis of stiffened samples, the level of difference between the full plate and each defects indexes is more than 50% with the C-scan method. Despite the defects values are always higher than reference zone with the calculated DIs too, the difference does not reach a minimum of 50% for most defects located in the 45° direction. The difference between each defect and the reference zone is satisfying for purposes of NDT in the case of SDI, but the importance of discrepancies between the values causes the standard deviation to be relatively high and therefore reduces the accuracy. It is also observed on each DI that the indexes measured in the 10 mm diameter defects is always smaller than in other defects, which confirms the possibility of size condition for defects detectability already mentioned in the previous part. Finally, the quantitative results also confirm the unability of Wave velocity DI to detect defects as most of the values are lower than the reference zone. Overall, the quantitative analysis of LW-16-00-siz confirms once again that the SDI is the best DI for defects detection.

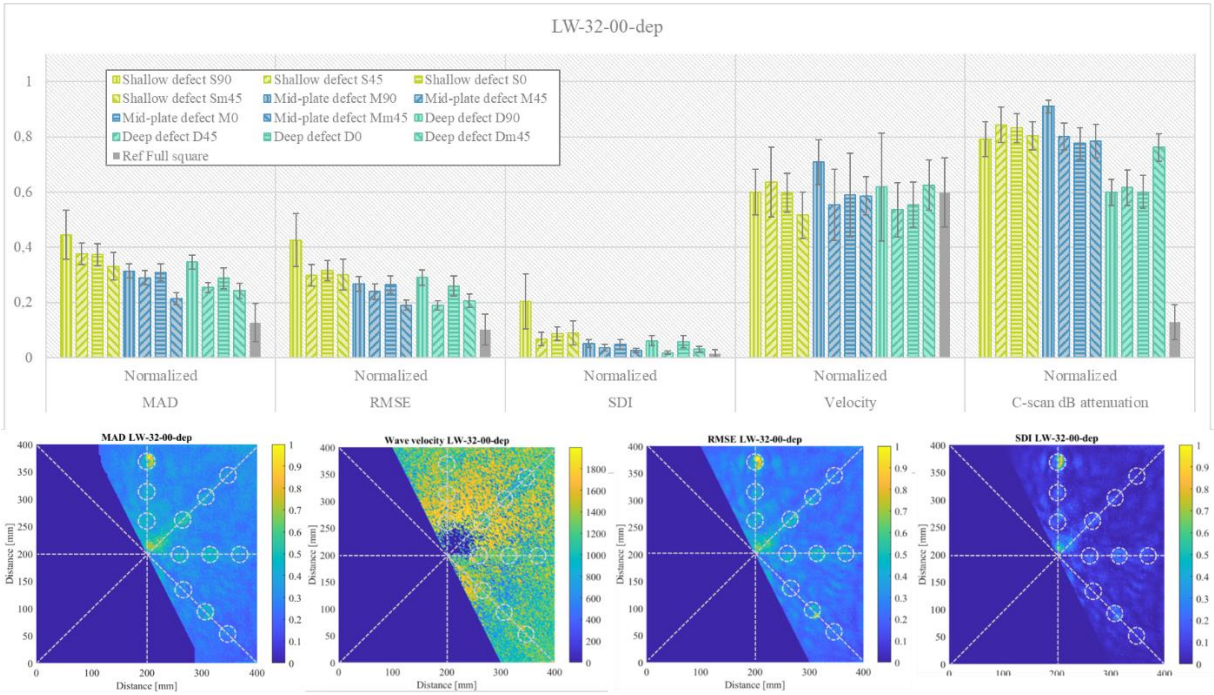

Figure 11: a) Quantitative and b) Qualitative results for LW-32-00-dep

The analysis of LW-32-00-dep quantitative results presented in figure 11 allow to obtain similar conclusions regarding the performance of Wave velocity and SDI indexes. Moreover, the effect of defect depth can be further interpreted. For each DI including the reference DI using C-scan but except the Wave velocity, the values for deeper defects are smaller than for other defects. However, whereas in the case of C-scan the difference between deep defects values and full plate is important enough to allow a clear detection of the defects, this difference is reduced in the case of calculated DIs in the current study. This is especially true for the case of SDI. Moreover, it is shown again that the discrepancy between every point of defects zones is high and generates important standard deviation which leads to less accuracy. This is clearly observed on the qualitative results with the spatial cartographies. The clear detection of the shallow defect on the 90° direction which is already visible on the cartographies is also confirmed with the MAD, RMSE and SDI quantitative results.

DISCUSSION AND CONCLUSION

In this study, a new method involving a fully non-contact system based on a LIPSW for Lamb Waves excitation and a novel Signal Processing algorithm adapted to this system is presented in the objective of proposing innovative ways of performing NDT in CFRP. The investigation performed, which is the first attempt of defects detection using this novel system, successfully validated the possibility of detecting artificial delamination. The Signal Processing method developed in this study consists in an algorithm containing three main steps: a Wavelet analysis, the parallel calculation of various Damage Indexes, some being based on Image Processing tools, and finally the optimization of a Probability Function allowing to visualize the probability of defects presence in the samples.

The results shown that the best Damage Index to characterize the samples inner structure is the Structural Dissimilarity Index. This is due to the fact that, as a global Image Processing tool which characterizes the main differences between control-line and baseline extracted images without taking into account small and punctual differences which are due to the measurement method inaccuracies, the SDI allows to emphasize only the important wave features generated by the presence of defects. However, the SDI also generates indications in highly disturbed zones such as the excitation zone, which could lead to a

wrong defect indication. Moreover, SDI such as other DIs shown unability to clearly size and localise some defects, in particular small defects and deep defects. Overall, this means that at this stage of the study, it is already possible to identify detectability conditions of the proposed method in terms of distance from the excitation point, size and depth of the defects. The thresholds will be quantified in the further studies.

Another limitation was observed in the case of stiffened samples which included wide delamination. The slight differences between healthy sample used as a baseline and defected samples used as control-lines leaded to disturbed zones in some healthy zones. In further studies, this issue will be attempted to be solved by implementing new baselines generated from numerical simulation.
Finally, another lead of improvement which will be investigated by the authors is the possibility to calculate other Damage Indexes based on other wave features which information are supposed to be contained in the 3D WT matrices. While this study allowed to confirm the possibility to detect artificial defects using a Signal Processing algorithm adapted to a fully non-contact Lamb Waves system, some further improvements will be investigated with the objective of obtaining a detection comparable to an ultrasonic C-scan control.

ACKNOWLEDGEMENTS

The authors thank the Japan Society for the Promotion of Science for their support under the Grant-in-Aid for Scientific Research programs (Grant No. JP22H01692).

REFERENCES

[1] Guo, N. & Cawley, P. (1993), The Interaction of Lamb Waves with delaminations in composite laminates, *J Acoust Soc Am*, 94(4), pp. 2240-2246.
[2] Kessler, S., Spearing, S. & Soutis, C. (2002), Damage Detection in Composite Materials using Lamb Waves methods, *Smart Mater Struct*, 11(2), pp. 269-278.
[3] De Luca, A., Sharif-Khodaei, Z., Aliabadi, M. and Caputo, F. (2016), Numerical Simulation of the Lamb Waves Propagation in impacted CFRP laminate, *Procedia Engineering*, 167, pp. 109-115.
[4] Kang, K., Chun, H., Son, J., Lee, J., Byun, J., Um, M., Lee, S. and Jang, J. (2011), Quantit tive accessibility of delamination in composite using Lamb Wave by experiments and FEA, *Adv Compos Mater*, 20(4), pp. 361-373.
[5] Castaings, M., and Cawley, P. (1996), The generation, propagation, and detection of Lamb waves in plates using air-coupled ultrasonic transducers, *J Acoust Soc Am*, 100(5), 3070–3077.
[6] An, Y. K., Park, B., & Sohn, H. (2013), Complete noncontact laser ultrasonic imaging for automated crack visualization in a plate. *Smart Mater Struct*, *22*(2).
[7] Toyama, N., Ye, J., Kokuyama, W., & Yashiro, S. (2018), Non-contact ultrasonic inspection of impact damage in composite laminates by visualization of Lamb wave propagation, *Applied Sciences (Switzerland)*, *9*(1).
[8] Yashiro, S., Takatsubo, J., Miyauchi, H., & Toyama, N. (2008), A novel technique for visualizing ultrasonic waves in general solid media by pulsed laser scan, *NDT&E Int*, 41(2), 137–144.
[9] Hosoya, N., Umino, R., Kanda, A., Kajiwara, I., & Yoshinaga, A. (2018), Lamb wave generation using nanosecond laser ablation to detect damage, *J Vib Control*, 24(24), 5842–5853.
[10] Lee, S. E., Liu, P., Ko, Y. W., Sohn, H., Park, B., & Hong, J. W. (2019). Study on effect of laser-induced ablation for Lamb waves in a thin plate. *Ultrasonics*, 91, 121–128.
[11] Hosoya, N., Yoshinaga, A., Kanda, A., & Kajiwara, I. (2018). Non-contact and non-destructive Lamb wave generation using laser-induced plasma shock wave. *Int J Mech Sci*, 140, 486–492.
[12] De Marchi, L., Perelli, A., & Marzani, A. (2013). A signal processing approach to exploit chirp excitation in Lamb wave defect detection and localization procedures. *Mech Syst Signal Pr*, 39(1–2), 20–31.
[13] Ramadas, C., Hood, A., Padiyar, J., Balasubramaniam, K., & Joshi, M. (2011). Sizing of delamination using time-of-flight of the fundamental symmetric Lamb modes. *J Reinf Plast Comp*, 30(10), 856–863.
[14] Waltisberg, D., Zurich, E., Raišutis, R., Waltisberg, D., & Raišutis, R. (2008). Group velocity estimation of Lamb waves based on the wavelet transform. *ULTRAGARSAS (ULTRASOUND)*, 63(4).
[15]] Feng, B., Ribeiro, A. L., & Ramos, H. G. (2018). A new method to detect delamination in composites using chirp-excited Lamb wave and wavelet analysis. *NDT&E Int*, 100, 64–73.